Computing Primitive of Fully VCSEL-Based All-Optical Spiking Neural Network for Supervised Learning and Pattern Classification

Shuiying Xiang, Zhenxing Ren, Ziwei Song, Yahui Zhang, Xingxing Guo, Genquan Han, and Yue Hao, *Senior Member, IEEE*

***Abstract*— We propose computing primitive for an all-optical spiking neural network (SNN) based on vertical-cavity surface-emitting lasers (VCSELs) for supervised learning by using biologically plausible mechanisms. The spike-timing-dependent plasticity (STDP) model was established based on the dynamics of the vertical-cavity semiconductor optical amplifier (VCSOA) subject to dual-optical pulse injection. The neuron-synapse self-consistent unified model of the all-optical SNN was developed, which enables reproducing the essential neuron-like dynamics and STDP function. Optical character numbers are trained and tested by the proposed fully VCSEL-based all-optical SNN. Simulation results show that the proposed all-optical SNN is capable of recognizing ten numbers by a supervised learning algorithm, in which the input and output patterns as well as the teacher signals of the all-optical SNN are represented by spatiotemporal fashions. Moreover, the lateral inhibition is not required in our proposed architecture, which is friendly to the hardware implementation. The system-level unified model enables architecture–algorithm codesigns and optimization of all-optical SNN. To the best of our knowledge, the computing primitive of an all-optical SNN based on VCSELs for supervised learning has not yet been reported, which paves the way toward fully VCSEL-based large-scale photonic neuromorphic systems with low power consumption.**

***Index Terms*— All-optical spiking neural network (SNN), neuromorphic photonics, spike-timing-dependent plasticity (STDP), supervised learning, vertical-cavity surface-emitting laser (VCSEL).**

I. Introduction

BRAIN-INSPIRED neuromorphic computing is a promising candidate for the next generation of intelligence computing. Even though modern processors based on the von Neumann architecture are capable of performing high-speed logic and scientific computations, they are poor in solving certain tasks, such as image recognition and natural language processing. One major limitation for conventional computers is the memory bottleneck, originating from the large latency, and energy consumption because of the physical separation between memory and computing units. Although the brain remains vastly unexplored, it is widely accepted that the brain adopts a colocated computing and storage strategy via a neurosynaptic framework [1], [2]. That is, it processes information in the location where it is stored without physically separating the computing and memory functions. It is also worth noting that the spatiotemporal processing in the brain is indispensable for the recognition of natural stimuli. In recent years, tremendous efforts have been directed toward brain-inspired spiking neural networks (SNNs) that are designed to closely emulate the architecture and functionality of biological nervous systems, and, hence, provide a more biologically plausible way to implement neuromorphic computing [3], [4]. In an SNN, information is encoded with spikes, which can lead to a very power-efficient computation and is well suited to describe the spatiotemporal processing inside the brain [5]–[7].

Over the past two decades, tremendous efforts from both the neuroscience community and the artificial intelligence community have been devoted to designing learning algorithms for software-based SNNs [8]–[40]. Research efforts are devoted to two main directions: unsupervised (without labeled data) and supervised (with labeled data) training by taking advantage of the timing information. Spike-timing-dependent plasticity (STDP), which is observed in biological synapses and is considered to be closely related to the learning mechanism, is a popular unsupervised learning rule [9]–[11], [15], [16], [30], [34]. It adjusts the synaptic weight according to the difference between presynaptic and postsynaptic spikes. When the presynaptic spike precedes in a specific time window (STDP window) the postsynaptic spike, the weight is potentiated and is depressed otherwise. For supervised machine learning, an SNN is first trained with examples from the field and then employed for inference with in-field data. There are also various famous algorithms for supervised learning in SNNs, such as SpikeProp [12], Tempotron learning rule [13], ReSuMe [17], SWAT [18], Chronotron [19], SPAN [20], and PSD rule [24]. In addition,

Manuscript received October 10, 2019; revised January 21, 2020 and March 28, 2020; accepted June 28, 2020. This work was supported in part by the National Key Research and Development Program of China under Grant 2018YFB2200500 and in part by the National Natural Science Foundation of China under Grant 61974177 and Grant 61674119. *(Corresponding author: Shuiying Xiang.)*

Shuiying Xiang is with the State Key Laboratory of Integrated Services Network, Xidian University, Xi'an 710071, China, and also with the State Key Discipline Laboratory of Wide Band Gap Semiconductor Technology, School of Microelectronics, Xidian University, Xi'an 710071, China (e-mail: syxiang@xidian.edu.cn).

Zhenxing Ren, Ziwei Song, Yahui Zhang, and Xingxing Guo are with the State Key Laboratory of Integrated Services Network, Xidian University, Xi'an 710071, China.

Genquan Han and Yue Hao are with the State Key Discipline Laboratory of Wide Band Gap Semiconductor Technology, School of Microelectronics, Xidian University, Xi'an 710071, China.

Color versions of one or more of the figures in this article are available online at http://ieeexplore.ieee.org.

Digital Object Identifier 10.1109/TNNLS.2020.3006263

the supervised learning algorithms for multilayer SNNs or deep SNNs have also gained increasing interest [27], [29], [31]–[33], [36], [38]. These supervised learning algorithms are mainly based on gradient descent, synaptic plasticity mechanism, or the convolution of spike trains [32]. Especially, the STDP mechanism has also been widely employed to design biologically plausible supervised learning [17], [33], [36], [39], [40]. For example, the ReSuMe rule proposed by Ponulak and Kasi' nski [17], which is originated from the Widrow–Hoff rule, is applicable to various types of spiking neuron models. It combines both STDP and anti-STDP processes and can learn precise spatiotemporal spikes patterns. Note that the majority of neural network algorithms are implemented on the computing systems based on the conventional von Neumann architecture. Consequently, we are not able to capitalize on the full benefit of SNNs. The current hardware implementation of a neural network algorithm is still far from competing with biological neural systems in terms of energy consumption.

To overcome these limitations, tremendous progress has been achieved in the SNN hardware, such as electronic neuromorphic computing system based on complementary metal–oxide–semiconductor (CMOS) technology and emerging memories [41]–[57]. They aim at mimicking the brain structure and computation in hardware. For instance, SpiNNaker [43], Neurogrid [44], TrueNorth [45], Loihi [56], and Tianjic [57] are emerging prototypical neuromorphic processors. Recently, Shastri *et al.* [58] compared comprehensively the performance of neuromorphic hardware platforms and highlighted that the neuromorphic photonic architectures potentially offered better speed-to-efficiency characteristics than state-of-the-art electronic counterparts. Hence, photonic implementation of hardware SNN offers a promising opportunity for ultrafast neuromorphic computing that complements electronic neuromorphic computing aimed at biological timescales due to its fascinating advantages, such as high speed, wide bandwidth, and massive parallelism [58]–[89]. However, photonics neuromorphic computing is in its early developmental stage compared with electronic counterparts.

In recent years, many photonic devices have been proposed to experimentally and numerically emulate the neuron-like spiking dynamics and the STDP function. The photonic neurons mainly include vertical cavity surface-emitting laser (VCSEL) [59], [60], [62], [67], [71]–[75], [79], [83], [88], micropillar laser with an integrated saturable absorber [63], [87], phase-change spiking neuron [75], [79], [81], [84], modulator-based neuron [80], [82], [85], and so on. In addition, the semiconductor optical amplifiers (SOA), the vertical-cavity SOA (VCSOA), and the phase-change material-based synapse are numerically and experimentally demonstrated to perform the STDP function [61], [64], [66], [68], [69], [78]. For instance, in 2013, Nahmias *et al.* [62] developed an analytical model for photonic neuron based on the VCSEL with an embedding saturable (VCSEL-SA). In 2019, an all-optical SNN with self-learning capacity consisting of 4 neurons and 60 synapses implemented on a nanophotonic chip has been reported, which provided a step toward optical neuromorphic systems that will benefit from the high-bandwidth and high-speed properties [84]. While a more detailed discussion is beyond the scope of this article, for recent work regarding the advances in photonic neuromorphic systems, we refer the readers to [67] and [82].

In our previous work, we developed a computational model of all-optical SNN for STDP-based unsupervised learning, by incorporating the plasticity model based on a VCSOA [86]. In that work, a single postsynaptic neuron (POST) would converge to the first spike timing of the input pattern through STDP-based unsupervised learning and could recognize only one spike pattern at a time, while, for more complex cognitive tasks, such as pattern classification, the winner-take-all, or lateral inhibition mechanisms, are usually required [16], [30], [34], [37], [40]. For instance, it has been demonstrated that the conventional STDP unsupervised learning rule could be improved by adding lateral inhibition and adaptive threshold [30]. On the other hand, it is widely agreed that supervised learning, which also existed in the brain, outperforms the unsupervised learning for certain tasks, such as pattern classification [40]. Note that, currently, even some novel attempts have been proposed to emulate the inhibitory dynamics of a spiking neuron in the optical domain, and the inhibitory synapse is still difficult to implement in the optical domain due to the absence of negative optical pulse [83], [90]–[92]. If extra optical–electrical–optical conversion units are introduced to realize the inhibitory connection, the circuit complexity will be increased substantially. That is to say, constructing an all-optical SNN with lateral inhibition remains a significant challenge. Hence, to improve the information processing capacity of all-optical SNN, a biological plausible supervised training method is highly desired. However, a versatile analytical model for all-optical SNN consisting of VCSELs and VCSOA for supervised learning is still lacking.

In this work, we present computing primitive for all-optical SNN for supervised learning, where VCSEL-SA and VCSOA are employed as photonic neurons and synapse, respectively. Our contribution is threefold. First, the rate equation model of VCSEL-SA and VCSOA subject to optical pulse injection is mathematically adapted to biologically plausible spiking neuron and STDP learning, which allows reproducing various neuron- and synapse-like dynamics. Second, we design a novel framework of a fully VCSEL-based all-optical SNN for supervised learning and classification tasks and develop a self-consistent unified neuron-synapse-learning model that allows a complete learning-to-inference workflow. Third, as the implementation of inhibition in the optical domain still remains a significant challenge, our proposed framework eliminates the inhibition requirement and, thus, offers a hardware-friendly approach in the implementation of SNN in the optical domain.

The rest of this article is organized as follows. In Section II, the architecture of the fully VCSEL-based all-optical SNN is described. The neuron-synapse self-consistent unified model of the all-optical SNN is also presented. Section III presents the dynamics of the all-optical neuron and plasticity property of the VCSOA. In Section IV, the supervised learning and recognition of spatiotemporal spike sequences are demonstrated in detail, and the classification tasks are performed. Furthermore, we consider a more biologically plausible spike

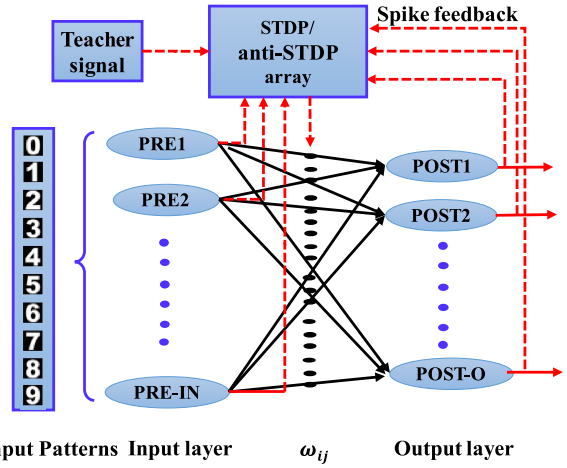

Fig. 1. Architecture of the proposed all-optical SNN. Spatiotemporal inputs and spatiotemporal outputs are considered; 0–9 are ten input patterns, PRE-1–PRE-IN represent the PREs based on VCSEL-SA, POST-1–POST-O denote the POSTs based on VCSEL-SA, and teacher signal is the target spikes. The training is performed by the ReSuMe method based on the STDP and anti-STDP rules.

encoding method by incorporating the convolutional operation for feature extraction to optimize the recognition rate. Finally, concluding remarks are provided in Section V.

II. Architecture and Model of All-Optical SNN

In this section, the hardware architecture of the proposed all-optical SNN is described first. The operation principle is introduced. Then, the unified theoretical model that characterizes the neuron and synapse dynamics is presented.

A. Hardware Architecture of the Proposed All-Optical SNN

All-optical SNN is a network that consists of optical spiking neurons. The architecture of the proposed all-optical SNN based on VCSELs is shown in Fig. 1. In an all-optical SNN, the input and output signals are expressed as spikes. The time interval for each training epoch is [0, T]. For supervised learning, both the input and teacher (supervisory) signals are applied to the all-optical SNN. The input pattern is first precoded into a stimulus rectangle pulse with different center timings. The stimuli pulses are then injected into the presynaptic neurons (PREs) to generate spikes with a time-based encoding scheme. Each PRE neuron is only allowed to fire a single spike. The spiking times are denoted as $t_{\text{pre}} = \{t_1, t_2, \ldots, t_{\text{IN}}\}$, where t_i is the spike time of the ith PRE. The spikes generated by the PREs are modulated by the photonic synapse and then are injected into each POST. Multiple spikes emission is allowed for each POST, and the spiking times of ten POSTs are denoted as $t_{\text{post}} = \{t_1^1, t_1^2, \ldots, t_1^{n_1}, t_2^1, t_2^2, \ldots, t_2^{n_2}, \ldots, t_O^1, t_O^2, \ldots, t_O^{n_O}\}$, where t_i^s is the timing of the sth spike generated by the ith POST. During each training epoch, the weight update is determined by the timing of the presynaptic spikes, postsynaptic spikes, and the supervisory spikes. The purpose of supervised learning is to make the POSTs emit at desired target timings.

To mimic the spatiotemporal information processing in the brain, spatiotemporal spikes are considered for the input signal, output signal, and the supervisory signal. More precisely, spatiotemporal coding contains information about space (in which neuron is spiking) and time (when a neuron is spiking).

B. Neuron-Synapse Self-Consistent Unified Model of the Proposed All-Optical SNN Based on VCSELs

Based on the architecture of the all-optical SNN, we adopt the VCSEL-SA as an optical spiking neuron. Note that the physics of an optical device, i.e., VCSEL-SA, is exploited to emulate a leaky-integrate-and-fire (LIF) model. We extend the rate equations of a VCSEL-SA by introducing the optical pulse injection to develop the model of the photonic neuron as follows [62], [86]:

$$\frac{dS_{i,o}}{dt} = \Gamma_a g_a (n_a - n_{0a}) S_{i,o} + \Gamma_s g_s (n_s - n_{0s}) S_{i,o} - \frac{S_{i,o}}{\tau_{\text{ph}}} + \beta B_r n_a^2 \tag{1}$$

$$\frac{dn_a}{dt} = -\Gamma_a g_a (n_a - n_{0a})\left(S - \Phi_{\text{pre},i} - \Phi_{\text{post},o}\right) - \frac{n_a}{\tau_a} + \frac{I_a}{eV_a} \tag{2}$$

$$\frac{dn_s}{dt} = -\Gamma_s g_s (n_s - n_{0s}) S_{i,o} - \frac{n_s}{\tau_s} + \frac{I_s}{eV_s} \tag{3}$$

$$\Phi_{\text{pre},i} = \frac{k_{ei}\tau_{ph}\lambda_i P_{ei}(\tau_i, \Delta\tau)}{hcV_a} \tag{4}$$

$$\Phi_{\text{post},o} = \sum_{i=1}^{n} \frac{\omega_i \lambda_i \tau_{ph} P_i(t - T)}{hcV_a} \tag{5}$$

$$P_{i,o}(t) \approx \frac{hc\eta_c \Gamma_a S_{i,o}(t) V_a}{\tau_{ph}\lambda_{i,o}}. \tag{6}$$

The subscripts a and s stand for the gain and absorber regions, respectively. $S_{i,o}$ represents the photonic density in the cavity. $n_a(n_s)$ denotes the carrier density in the gain (absorber) region. Equation (4) exists only for the PRE neuron, which represents the stimulus pulse. k_{ei}, τ_i, $\Delta\tau$ are stimuli strength, center timing, and temporal duration, respectively. For simplicity, we consider $k_{ei} = 10\ \mu w$, $\Delta\tau = 2$ ns, $\Delta\tau_i = 0.2$ ns. $I_s = 0$ mA, and $I_a = 2$ mA represent the bias current for the gain and absorber regions of VCSEL-SA, respectively. The spikes generated by PREs are all modulated by the synapse and then propagated to the POST. Equation (5) exists only for the POST, which characterizes the weighted summation. ω_i, which is the analog connection strength between VCSEL-SAs, represents the synaptic weight. In practice, ω_i can be tuned during training by a variable optical attenuator that is a passive optical component. Note that the dynamical isomorphism between the semiconductor photon carriers and the neuron biophysics is exploited here to reproduce the neuron-like dynamics. More precisely, the dynamics of the carriers n_a governed by (2) emulates the membrane potential of a LIF neuron, and P expressed in (6) that is proportional to the photon density S mimics the firing spike of a LIF neuron. The term Φ described by (4) and (5) denotes the stimulation. The external stimulation perturbs the carriers and triggers the VCSEL-SA that emits a photonic excitable spike when the carriers n_a exceed the threshold.

To obtain a unified system-level model of the all-optical SNN and understand the complex dynamical interaction of optical neuron and optical synapse, the rate equations of the optical neuron should be solved self-consistently with the equations of the synapse. The outputs of the PREs and POSTs are injected into the optical synapse. The STDP is implemented in a VCSEL operating below threshold (referred to as VCSOA). By injecting dual-optical spike with different central timings into the VCSOA, the model of a photonic synapse can be modeled by [78], [86], [93]–[98]

$$\frac{dN}{dt} = \frac{\eta I}{e\Gamma_1 V} - \left(AN + BN^2 + CN^3\right) - \frac{ca(N-N_0)}{n_c}\left(\beta_{sp}\overline{S}_{\text{ase}} + \overline{S}_i + \overline{S}_o\right) \tag{7}$$

$$\overline{S}_{i,o} = \left(\frac{(1-R_t)(1+R_bG_s)(G_s-1)}{\left(1-\sqrt{R_tR_b}G_s\right)^2 + 4\sqrt{R_tR_b}G_s\sin^2\Phi_{i,o}}\right) \times \frac{P_{i,o}n_c\lambda_p}{hc^2Vg} \tag{8}$$

$$G_{Ri,Ro} = \frac{\left(\sqrt{R_t}-\sqrt{R_b}G_s\right)^2 + 4\sqrt{R_tR_b}G_s\sin^2\Phi_{i,o}}{\left(1-\sqrt{R_tR_b}G_s\right)^2 + 4\sqrt{R_tR_b}G_s\sin^2\Phi_{i,o}} \tag{9}$$

$$P_{A_i,Ao}(t) = P_{i,o}(t)G_{Ri,Ro} \tag{10}$$

where $G_s = e^{[\Gamma_1 a(N-N_0)-\alpha_i]L_c}$, $\Phi_{i,o} = \Phi_{0i,0o} - b\Gamma_1 L_c a(N - N_s)/2$, and $\Phi_{0i,0o} = 2\pi n_c L_c(1/\lambda_{i,o} - 1/\lambda_p)$. N denotes the carrier density in the VCSOA. $\overline{S}_{\text{ase}}$ stands for the averaged spontaneous photon density. $\overline{S}_{i,o}$ means the averaged stimulated photonic density related to the PRE spike and POST spike, respectively. $G_{Ri,Ro}$ denote the amplifier gain. $P_{A_i,Ao}$ describe the amplified spikes power. $I = 5.8$ mA is the bias current of VCSOA.

Then, the STDP curve can be calculated by [78], [86]

$$\Delta\omega_{\text{STDP}}(\Delta t) = (P_{Ai\max} - \max[P_{Ai}(t)])/P_{Ai\max}, \quad \text{if } \Delta t = t_i - t_o > 0 \tag{11}$$

where $P_{Ai\max}$ is the maximum peak power for all the considered Δt, and $\max[P_{Ai}(t)]$ represents the peak power for a given Δt. The calculated $\Delta\omega_{\text{STDP}}(\Delta t)$ mimics the STDP mechanism of a biological synapse.

C. Learning Algorithm

The training process is implemented by the STDP-based ReSuMe supervised learning method [17]

$$\Delta\omega_i = \omega_f \times \left[(m_d - m_o) + \sum_{t_d}\sum_{t_i \le t_d}\Delta\omega_{\text{STDP}}(t_d - t_i) + \sum_{t_o}\sum_{t_i \le t_o}\Delta\omega_{a\text{STDP}}(t_o - t_i)\right], \quad \text{if } |t_o - t_d| > r \tag{12}$$

$$\omega_i(x+1) = \omega_i(x) + \omega_f \times \Delta\omega_i. \tag{13}$$

$\Delta\omega_i$ represents the weight update amount. Two processes are an STDP process for potentiating synapses based on input spike trains and desired target spikes and an anti-STDP process for depressing synapses based on the input spike trains and actual output spikes. Note that the anti-STDP is simply calculated by $\Delta\omega_{a\text{STDP}}(\Delta t) = -\Delta\omega_{\text{STDP}}(\Delta t)$. $m_{d,o}(t_{d,o})$ denotes the number (time) of the desired target spikes and output spikes. ω_f is the learning rate. For a pattern recognition task, we assume that the recognition is successful when $|t_o - t_d| < r$ is satisfied, where $t_o(t_d)$ denotes the output (target) spike timing. In this work, we consider $r = 0.5$ ns. The other typical parameters and the values for both the optical neuron and synapse models are summarized in Table I.

TABLE I

SOME TYPICAL PARAMETERS OF VCSEL-SA AND VCSOA IN THE ALL-OPTICAL SNN USED IN SIMULATION [86], [95]. THE SUBSCRIPTS a AND s STAND FOR THE GAIN AND ABSORBER REGIONS, RESPECTIVELY

Description	Param and value
Top and bottom DBR reflectivity	$R_t = 0.99, R_b = 0.995$
Cavity refractive index	$n_c = 3.3$
Cavity volume	V=3.86×10^{-17}m^3
Peak wavelength of VCSOA	λ_p=845.58nm
Effective cavity length	$L_c = 3\lambda_p / n_c$
Linewidth enhancement factor	$b = 2.7$
Linear material gain coefficient	$a = 2.48\times10^{-20}$m^2
Average cavity loss coefficient	$\alpha_i = 1165$m^{-1}
Internal quantum efficiency	$\eta = 0.4$
Longitudinal confinement factor	$\Gamma_1 = 0.1$
Nonradiative recombination rate	$A = 1\times10^8 s^{-1}$
Radiative recombination coefficient	$B = 1\times10^{-16}$m$^6 s^{-1}$
Auger recombination coefficient	$C = 5\times10^{-42}$m$^6 s^{-1}$
Spontaneous emission factor	$\beta_{sp} = 2.5\times10^{-5}$
Transparency carrier density	$N_0 = 2\times10^{24}$m^{-3}
Wavelength of PREs (POSTs) VCSEL-SA	λ_i = 845.58nm , λ_o = 845.57nm
Differential gain/loss	$g_a = 2.9\times10^{-12}$ m^{3}s^{-1} , $g_s = 14.5\times10^{-12}$ m^{3}s^{-1}
Cavity volume	$V_{a,s} = 2.4\times10^{-18}$m^3
Carrier lifetime	τ_a = 1ns, τ_s = 100ps
Photon lifetime of VCSEL-SA	$\tau_{\text{ph}} = 4.8$ps
Transparency carrier density	$n_{0a} = 1.1\times10^{24}$ m^{-3} $n_{0s} = 0.89\times10^{24}$ m^{-3}
Bimolecular recombination term	$B_r = 10\times10^{-16}$m^{3}s^{-1}
Spontaneous emission coupling factor	$\beta = 1\times10^{-4}$
Confinement factor	$\Gamma_a = 0.06, \Gamma_s = 0.05$
Output power coupling coefficient	$\eta_c = 0.4$

III. DYNAMICS OF ALL-OPTICAL NEURON AND STDP

To begin with, we present a brief description of the neuron- and synapse-like dynamics. The excitability properties and the spike latency of the PREs are considered. We define the timing corresponding to the maximum value of spikes generated by PRE as t_i. Fig. 2 shows the temporal outputs of the different PREs that are subjected to rectangle stimuli pulses with different stimuli strengths and central timings. We define

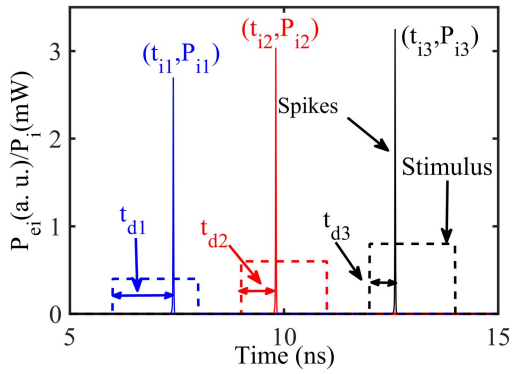

Fig. 2. Temporal output of the spike encoding based on the modeling-based photonic neuron. Larger stimuli strength leads to higher output spike powers and smaller spike latency (spike to the onset of stimuli) $t_{d1} > t_{d2} > t_{d3}$.

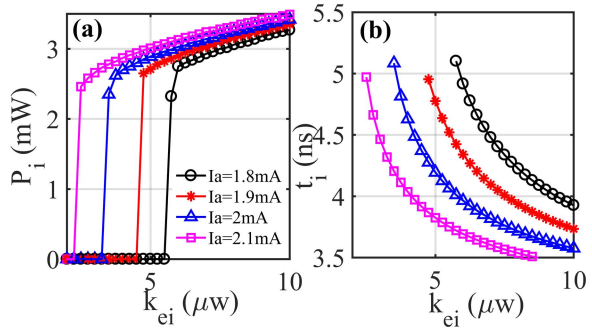

Fig. 3. (a) Threshold-like response and (b) spike latency property of the modeling-based photonic neuron. P_i and t_i are spike power and timing for the PRE neuron.

the timing corresponding to the maximum value of spikes as t_i. The interval between the start time of stimulus pulse and t_i is denoted as spike latency t_{di}. As we can clearly see from Fig. 2, for the stimuli strength $k_{\mathrm{e3}} > k_{\mathrm{e2}} > k_{\mathrm{e1}}$, the spike latency values satisfy $t_{\mathrm{d1}} > t_{\mathrm{d2}} > t_{\mathrm{d3}}$. The spike power P_i and spike timing t_i as functions of the stimuli pulse power k_{ei} for the different I_a are presented in Fig. 3. It is obvious that when k_{ei} exceeds a threshold value, the PRE emits a spike. A larger I_a leads to a smaller threshold value of k_{ei}. Besides, above the threshold, a larger k_{ei} leads to higher (smaller) $P_i(t_i)$. These results are in accordance with the experiment findings [63].

In biological systems, POSTs emit spikes when the membrane voltage reaches the firing threshold. Next, we consider the spiking dynamics of the POST that is subjected to a train of spikes injection that coming from the PREs with a fixed time interval $\Delta\tau_i = 0.2$ ns. Fig. 4 shows the time series of PRE spikes, the carrier density in the gain region of POST n_{ao}, and the POST spikes. It can be found that when a PRE spike arrives, n_{ao} increases sharply and exceeds the threshold. The POST emits a spike immediately, which is followed by the quick decay of n_{ao} to the rest state. This reset acts as a refractory mechanism since the POST must reach the firing threshold from the rest state to fire again. That is to say, the dynamics of n_{ao} is similar to the excitatory postsynaptic potential (EPSP). As can be seen in Fig. 4(c), the POST cannot emit another spike, even if it further receives the PRE spikes in a short time. After that, the EPSP reaches the threshold again by receiving a train of five PRE spikes, and the POST

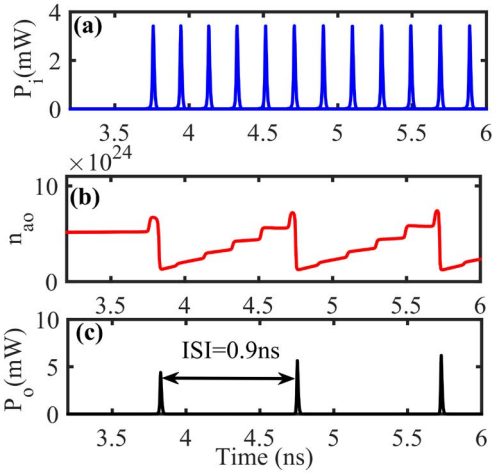

Fig. 4. (a) Presynaptic spikes, (b) carrier density in the POST, and (c) postsynaptic spike outputs, with $\Delta\tau_i = 0.2$ ns, $\Delta\tau = 2$ ns, and $\omega_0 = 0.1$.

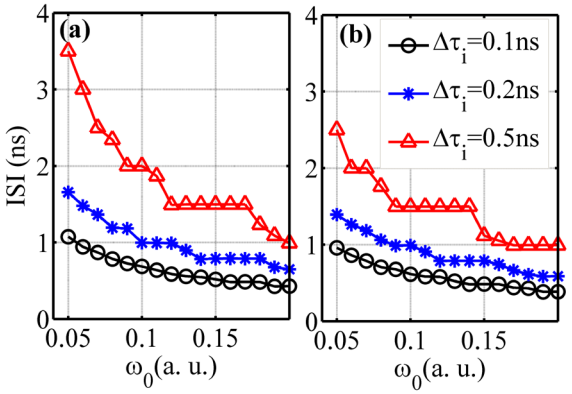

Fig. 5. ISI of the POST as a function of ω_0 under different $\Delta\tau_i$ for (a) $I_a = 1.8$ mA and (b) $I_a = 2$ mA. ISI is decreased (increased) with ω_0 ($\Delta\tau_i$) and is slightly smaller for a larger Ia when ω_0 is relatively small.

emits a spike. The interspike interval (ISI) is 0.9 ns, which mimics the refractory period of a neuron.

For the POST, the dependence of ISI on the initial weight ω_0 is further presented in Fig. 5. It is obvious that the ISI decreases with ω_0, while increases with $\Delta\tau_i$. Besides, for relatively small ω_0, a larger I_a leads to a smaller ISI. Note that a smaller ISI indicates a higher spiking processing speed [88].

Based on the model of a VCSOA subject to dual-optical spike injection, as presented in (7), the calculated STDP curves according to (11) for different bias current of VCSOA are presented in Fig. 6. The bias current ranges from 5.5 to 6.3 mA. It is found that when the PRE spike arrives early, i.e., $\Delta t = t_o - t_i > 0$, the weight is potentiated ($\Delta\omega > 0$). Otherwise, weight is depressed ($\Delta\omega < 0$). The STDP curve is similar to the STDP response in a biological synapse [10] and is also similar to the experimental measurements for the conventional SOA [64], [68], [69]. It is obvious that the height and width of the STDP window can be finely tuned by the bias current. For convenience, we consider the STDP and anti-STDP windows as 2 ns when designing the supervised learning algorithm in the following.

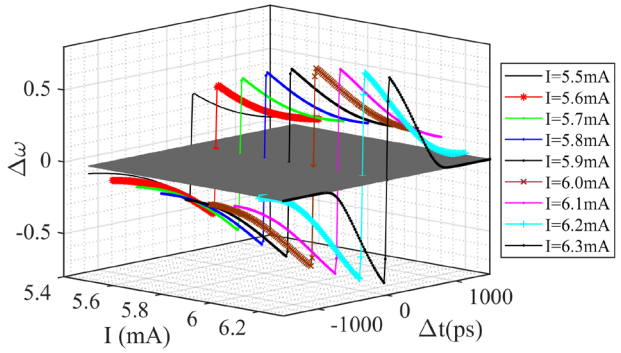

Fig. 6. Calculated STDP curves for different I's. The STDP curves corresponding to I ranging from 5.5 to 6.3 mA, as denoted by the legends (from left to right).

IV. Supervised Learning and Pattern Recognition

In order to view the functionality of the fully VCSEL-based all-optical SNN, we created an algorithm-device-circuit framework and tested on spike sequence learning and optical character recognition (OCR) tasks. The architecture of the all-optical SNN is a fully connected network. The performances are presented in the following.

A. Spike Sequence Learning

Before we demonstrate the classification task, we first consider a simple spike sequence learning by using a single POST. The purpose of spike sequence learning is to train the network to map a spatiotemporal input into a determined spike sequence. For simplicity, in the first group of experiments, the number of PREs is set to 220, and the number of POST is 1. For the mth PRE, the central time of the rectangle stimulus pulse is precoded as follows:

$$t_e(m) = [6 + \Delta\tau_i \times m] \text{ ns}, \quad \text{with } \Delta\tau_i = 0.1 \text{ ns}. \tag{14}$$

The target timing of the POST is predefined as follows:

$$t_d = [10 \text{ ns}, 12 \text{ ns}, 14 \text{ ns}, 16 \text{ ns}, 18 \text{ ns}, 20 \text{ ns}, 22 \text{ ns}, 24 \text{ ns}, 26 \text{ ns}, 28 \text{ ns}]. \tag{15}$$

Note that the ISI of the target spike strain is set to be equal to the STDP window defined earlier. For the purpose of faster convergence performance, the number of input spikes involved in each target time is suggested to be similar. Hence, the start time and end time of the input spike should be carefully chosen according to the STDP window and the detailed target time. We present a simple schematic of the STDP window in our learning algorithm in Fig. 7. Here, each input spike comes from one PRE, and the time interval of two consecutive spikes from two different PREs is $\Delta\tau_i = 0.1$ ns. The target is a period spike train, and the periodicity is $\Delta\tau_d = 2$ ns. The output is a sequence of period spike with periodicity being the ISI, as shown in Figs. 4 and 5. According to (12), the weight update amount is $\Delta\omega_1 = \omega_f \times [(m_d - m_o) + \omega^1_{\text{STDP}} + \omega^1_{a\text{STDP}} + \omega^2_{a\text{STDP}}]$, as can be seen from the schematic of the weight in Fig. 7.

When the input patterns are repeatedly fed into all-optical SNN during the training process, the weights are updated according to the ReSuMe method. To obtain faster training

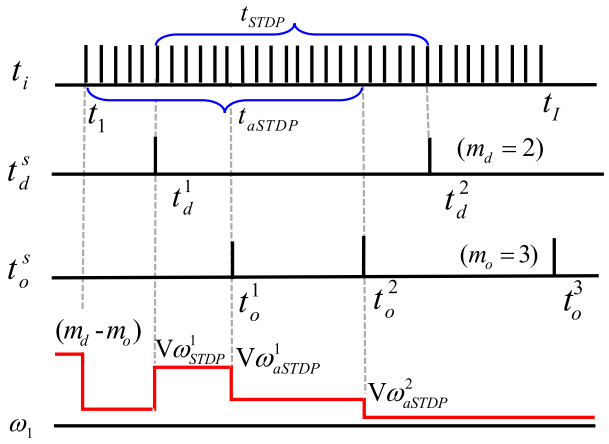

Fig. 7. Input spikes, desired target, and actual output spikes during a running process, and the weight update diagram (from top to bottom). Both the STDP and anti-STDP windows are set as 2 ns.

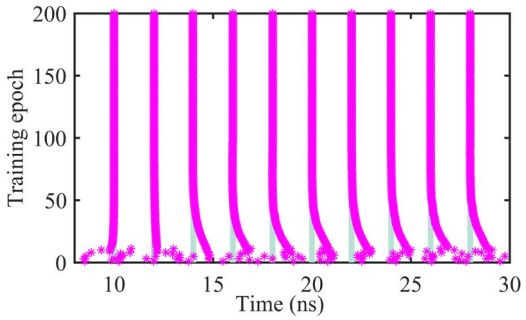

Fig. 8. Training process of spike sequence learning of a single POST. (The target spike sequence is denoted by the light green bars.)

convergence, we considered that the spike sequence is correctly learned if the spike time difference between each pair of output and target spike is less than 20 ps. Namely, the weights are not updated if $|t_o - t_d| < 20$ ps is satisfied for all the ten pairs of output-target spikes. The initial synaptic weights are set as $\omega_i(0) = 0.02 \times [(2 \times \xi - 1) \times 0.2 + 1]$, where ξ is a random number with uniform distribution generated by the MATLAB function rand(1, 220). The learning rate is set as $\omega_f = 0.004$. The timing of the POST spikes during the training process is presented in Fig. 8. It can be seen that at the beginning, the output spike sequence is different from the target sequence. After several training epochs, the POST emits spikes at the desired targets timing as predefined timing, indicating that the learning is converged. To obtain statistical significance, we repeat the spike sequence learning task 100 times. The distribution for the initial weights, as well as the weights after convergence, is illustrated in Fig. 9. It can be seen that the initial weights shown in Fig. 9(a) are uniformly distributed around 0.02, which indicates that there are no significant differences among the synaptic weight. After training 200 epochs, the synapses corresponding to presynaptic spike time close to the time of target spikes are potentiated, while others are depressed. Namely, the modulation behavior of the weight can be clearly observed from Fig. 9(b), which shows training convergence. Hence, we can conclude that all-optical SNN is capable of spike sequence learning. We have also considered other cases of spike sequence learning. It is found

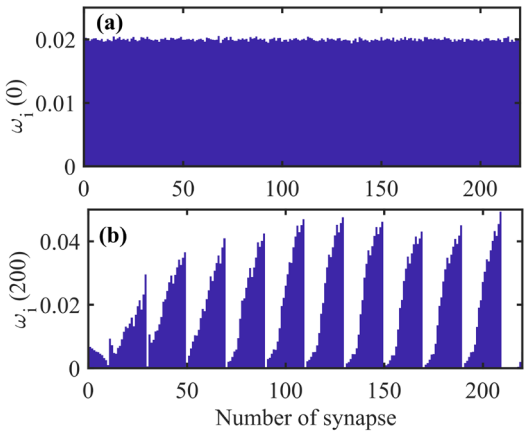

Fig. 9. (a) Averaged initial weights. (b) Averaged weights after convergence. The height of each bar corresponds to the weight. All the values are averaged over 100 repeated tests.

Fig. 10. (a) Clean character image and (b) noisy patterns.

that if the input spike timing, the STDP window, and the target timing are properly selected, the spike sequence learning can be realized successfully. Note that the number of PREs is suggested to be changed according to the number of target spikes.

B. Spatiotemporal Pattern Classification

Subsequently, we consider a pattern classification task, i.e., OCR. The all-optical SNN is composed of 400 PREs and ten POSTs. The network is trained with a clean character image, and then, the inference was tested with a set of noisy patterns, as shown in Fig. 10. The numbers "0"–"9" are considered as ten different input patterns. Each pattern is an image of size 20×20 pixels. Each pixel is encoded with a PRE neuron that allows single spike emission.

To ensure successful learning, the spatiotemporal encoding should provide enough spikes during the whole encoding window. To this end, we consider random encoding. For simplicity, the central timing of stimulus pulse for each PRE is determined by the pixel index m, pixel intensity $\mathrm{I}(m)$, and

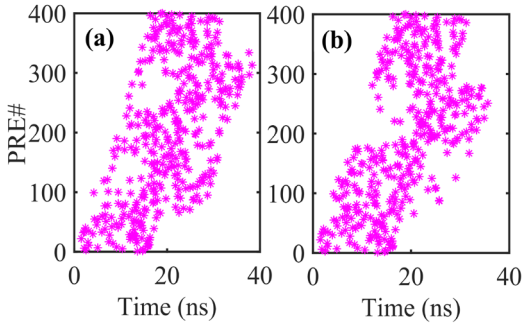

Fig. 11. Spatiotemporal coding spikes of numbers (a) 0 and (b) 1.

a random term $\mathrm{R}(m)$ as follows:

$$t_e(m) = [m + \mathrm{I}(m) + \mathrm{R}(m)] \times 0.04 \text{ ns}. \tag{16}$$

The spatiotemporal spike encoding for two representative patterns ("0" and "1") is presented in Fig. 11. It is obvious that the two patterns are encoded into different distributions of the spikes. All the PRE spikes are propagated to ten POSTs.

The spatiotemporal pattern of targets is defined as (17), shown at the bottom of the page.

Here, one raw represents one pattern, each column denotes a POST. For instance, for the Pattern "0," the target time is 10 ns for the POST1 and 40 ns for the rest nine POSTs. For the Pattern "1," the target time is 12 ns for the POST2, 40 ns for the rest nine POSTs, and so on. Namely, each pattern is cooperatively recognized by the ten POSTs. As will be demonstrated later, with the spatiotemporal design of the target, the lateral inhibition that is usually employed in pattern recognition [16], [30], [34] is no longer required to obtain a successful classification. Note that in the current stage of photonic neuromorphic, the hardware implementation of inhibition connection in the optical domain still remains a significant challenge due to the absence of a negative optical pulse. Hence, the spatiotemporal design of spike encoding in the proposed framework eliminates the inhibition requirement and enables hardware implementation of all-optical SNN with reduced circuit complexity.

The temporal evolution of the output spike timings during the training process is presented in Fig. 12. Here, ten patterns are trained separately in parallel. For simplicity, only the evolutions of POST1, POST2, and POST10 are given for Pattern "0." For the rest of the patterns, only one key POST is presented. It can be seen that for the pattern "0," after several

$$t_d = \begin{bmatrix} 10\text{ ns}, & 40\text{ ns}, & 40\text{ ns}, & 40\text{ ns}, & 40\text{ ns}, & 40\text{ ns}, & 40\text{ ns}, & 40\text{ ns}, & 40\text{ ns}, & 40\text{ ns}; \\ 40\text{ ns}, & 12\text{ ns}, & 40\text{ ns}, & 40\text{ ns}, & 40\text{ ns}, & 40\text{ ns}, & 40\text{ ns}, & 40\text{ ns}, & 40\text{ ns}, & 40\text{ ns}; \\ 40\text{ ns}, & 40\text{ ns}, & 14\text{ ns}, & 40\text{ ns}, & 40\text{ ns}, & 40\text{ ns}, & 40\text{ ns}, & 40\text{ ns}, & 40\text{ ns}, & 40\text{ ns}; \\ 40\text{ ns}, & 40\text{ ns}, & 40\text{ ns}, & 16\text{ ns}, & 40\text{ ns}, & 40\text{ ns}, & 40\text{ ns}, & 40\text{ ns}, & 40\text{ ns}, & 40\text{ ns}; \\ 40\text{ ns}, & 40\text{ ns}, & 40\text{ ns}, & 40\text{ ns}, & 18\text{ ns}, & 40\text{ ns}, & 40\text{ ns}, & 40\text{ ns}, & 40\text{ ns}, & 40\text{ ns}; \\ 40\text{ ns}, & 40\text{ ns}, & 40\text{ ns}, & 40\text{ ns}, & 40\text{ ns}, & 20\text{ ns}, & 40\text{ ns}, & 40\text{ ns}, & 40\text{ ns}, & 40\text{ ns}; \\ 40\text{ ns}, & 40\text{ ns}, & 40\text{ ns}, & 40\text{ ns}, & 40\text{ ns}, & 40\text{ ns}, & 22\text{ ns}, & 40\text{ ns}, & 40\text{ ns}, & 40\text{ ns}; \\ 40\text{ ns}, & 40\text{ ns}, & 40\text{ ns}, & 40\text{ ns}, & 40\text{ ns}, & 40\text{ ns}, & 40\text{ ns}, & 24\text{ ns}, & 40\text{ ns}, & 40\text{ ns}; \\ 40\text{ ns}, & 40\text{ ns}, & 40\text{ ns}, & 40\text{ ns}, & 40\text{ ns}, & 40\text{ ns}, & 40\text{ ns}, & 40\text{ ns}, & 26\text{ ns}, & 40\text{ ns}; \\ 40\text{ ns}, & 40\text{ ns}, & 40\text{ ns}, & 40\text{ ns}, & 40\text{ ns}, & 40\text{ ns}, & 40\text{ ns}, & 40\text{ ns}, & 40\text{ ns}, & 28\text{ ns}; \end{bmatrix} \tag{17}$$

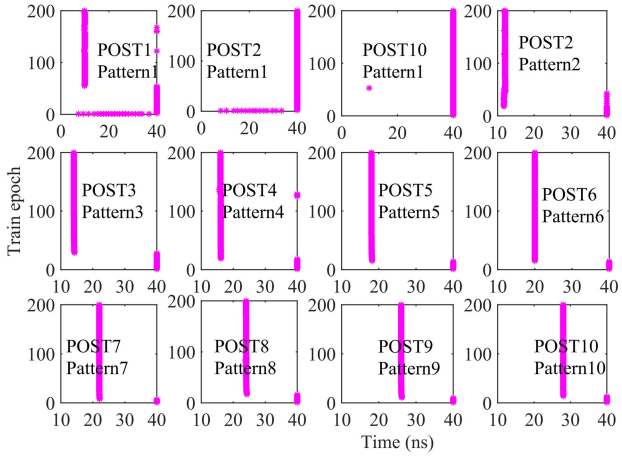

Fig. 12. Temporal evolution of the output spikes during the training process.

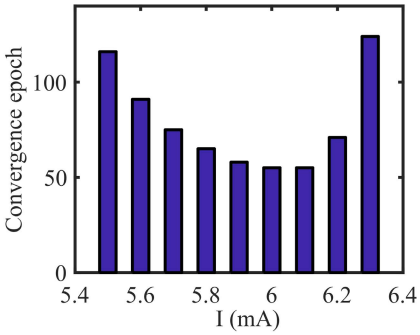

Fig. 13. Comparison of convergence performance for supervised learning with different I's. The convergence criterion is defined as $E_{\mathrm{VP}} < 0.5$.

training epochs, the POST1 emits spikes at 10 ns, while the rest POSTs emit spikes at 40 ns. For the rest patterns, the POSTs also emit spike at the predefined target timings after convergence. It is obvious that different input patterns can be classified successfully via supervised learning based on the all-optical SNN even without lateral inhibition.

To optimize the all-optical SNN to obtain faster training convergence, we modified the Victor & Purpura (VP) distance to quantify the spike distance between actual and target timings. The modified VP distance can be expressed as follows [19], [99]:

$$E_{\mathrm{VP}} = \sum_{m_o>1,|t_o^f-t_d|>r} 1 + \sum_{m_o=0} 1 + \sum_{m_o=1,|t_o-t_d|>r} 1 + \sum_{m_o=1,|t_o-t_d|<r} \frac{(t_o-t_d)}{\tau_f}. \quad (18)$$

The first term indicates that the number of spikes generated by a given POST is larger than 1. The second term represents that the given POST emits no spike. The third term means that the spike number of the actual output and target is the same, but the spiking timing difference is larger than r. The last term is the expected case. That is, the spike number of the actual output and target output is the same, and the difference between the target spiking timing and actual spike timing is less than r. $\tau_f = 1$ ns is a fitting parameter. For convenience, we consider $E_{\mathrm{VP}} < 0.5$ as the convergence criterion. The minimal training epoch leads to $E_{\mathrm{VP}} < 0.5$, which is regarded as the convergence epoch. Note that each

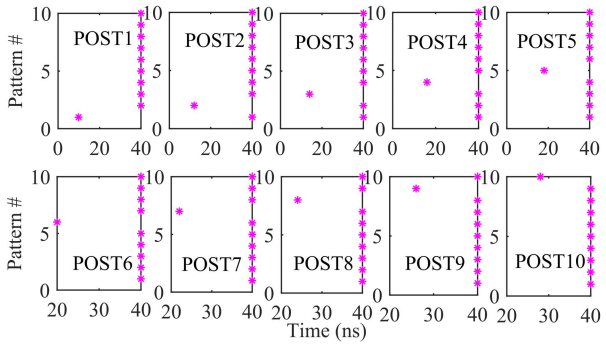

Fig. 14. Raster plots of testing ten patterns for ten POSTs with a clean pattern.

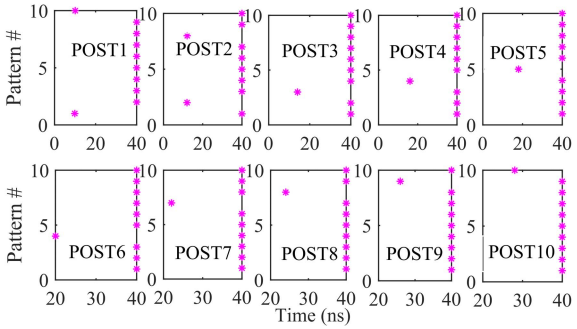

Fig. 15. Raster plots of testing ten patterns for ten POSTs with a noisy pattern.

pattern is corecognized by ten POSTs, and $E_{\mathrm{VP}} < 0.5$ should be satisfied for all the POSTs.

We now discuss how the operating parameters impact the application-level tasks and performance. The convergence epoch for different I of VCSOA is presented in Fig. 13. It is clear that the training process can be optimized by careful choice of I. Here, when $I = 6.1$ mA, the defined convergence criterion can be satisfied at the 53th epoch, which represents the best training performance.

After the training process is finished, the weight matrix is fixed. By feeding the clean pattern into the all-optical SNN, the inference process is performed with the trained weight. Fig. 14 shows the raster plots of ten POSTs for ten different patterns. For each pattern, the ten POST emit spikes at exactly the target timing. For instance, for Pattern "0," POST 1 emits at 10 ns, and POSTs 2–10 emit at 40 ns. For Pattern "1," POST2 emits at 12 ns, the rest POSTs emit at 40 ns, and so on. Namely, by using the trained weight, the patterns can be classified accurately.

We also consider noisy images in the testing phase. The noise is introduced as

$$\mathrm{noise} = \mu + \sigma \times \mathrm{randn}(20, 20). \quad (19)$$

That is, the noise matrix is added to the pixel matrix of the clean image. For $\mu = 0, \sigma = 0.5$, the raster plots are presented in Fig. 15. It can be seen that for Pattern "0," POST 1 emits at 10 ns, and POSTs 2–10 emit at 40 ns. For Pattern "1," POST 2 emits at 12 ns, and the rest nine POSTs emit at 40 ns. For Pattern "2," POST 3 emits at 14 ns, and the rest nine POSTs emit at 40 ns. Namely, these three patterns are correctly recognized. For Pattern "3," POST 4

emits at 16 ns, POST 6 emits at 20 ns, and the rest eight POSTs emit at 40 ns. That is to say, the Pattern "3" is not recognized successfully. Similarly, Patterns "5," "7," and "9" are not successfully identified. Hence, for these noisy patterns, six patterns can be correctly recognized.

To obtain the statistical significance of the inference accuracy rate, for each noise level, we run the test process 50 times. For each time, the noisy image is generated independently. Here, we define that the kth running test for pattern p is correct if $\max(E_{\mathrm{VP}}^{o}) < r$, that is, ten POSTs satisfy $E_{\mathrm{VP}} < 0.5$. Namely

$$C_k^p = \begin{cases} 1, & \max\left(E_{\mathrm{VP}}^{o}\right) < r, \quad o = 1, 2, \ldots, 10 \\ 0, & \text{otherwise.} \end{cases} \tag{20}$$

Then, the accuracy rate is calculated by

$$\text{Accuracy rate} = \frac{1}{K \times P} \sum_{k=1}^{K} \sum_{p=1}^{P} C_k^p. \tag{21}$$

Here, $K = 50$ means the total running test for each pattern, and $P = 10$ indicates the number of patterns. The dependence of the accuracy rate is presented in Fig. 16. It is clear that when the noise level is 0.2 or 0.4, the accuracy rate is close to 1. When the noise level is increased further, the accuracy rate is decreased almost linearly with the noise level and is close to 0.5 when $\sigma = 2$

$$C_{7\times7} = \begin{bmatrix} 1 & 1 & 4 & 1 & 1 & 1 & 8 \\ 1 & 1 & 1 & 1 & 2 & 1 & 1 \\ 1 & 128 & 1 & 1 & 1 & 1 & 16 \\ 1 & 32 & 1 & 1 & 1 & 1 & 1 \\ 1 & 1 & 1 & 1 & 1 & 64 & 1 \\ 1 & 1 & 1 & 256 & 1 & 1 & 1 \\ 1 & 1 & 1 & 1 & 1 & 1 & 1 \end{bmatrix}. \tag{22}$$

In the following, we also consider a more biological plausible spike encoding method similar to the visual system in the brain, as shown in Fig. 17. We consider two prior determined fixed convolutional filters as follows: one with the kernel size of 7×7, as presented in (22), and the other kernel is of size 5×5, as shown in (23). After the convolution operation, the sizes of the feature map are 14×14 and 16×16, respectively. Each element of the feature maps is transformed into a single spike of a PRE. Hence, the number of PREs is $14 \times 14 + 16 \times 16 = 452$

$$C_{5\times5} = \begin{bmatrix} 1 & 1 & 1 & 2 & 1 \\ 4 & 1 & 8 & 1 & 1 \\ 1 & 16 & 1 & 1 & 32 \\ 1 & 1 & 64 & 1 & 1 \\ 1 & 1 & 1 & 128 & 1 \end{bmatrix}. \tag{23}$$

Then, each pixel value is converted into a constant stimulus timing to perform spatiotemporal encoding as

$$t_C(j) = \frac{M(j)}{M_{\max}} \times T + 5 \text{ ns}, \quad j = 1, \ldots, 452 \tag{24}$$

where $t_C(j)$ is the spike time of the jth PRE neuron, $M(j)$ is the corresponding pixel intensity, $M_{\max}$ is the maximum intensity of all pixels, and $T = 35$ ns. The simulation time for each epoch is 40 ns.

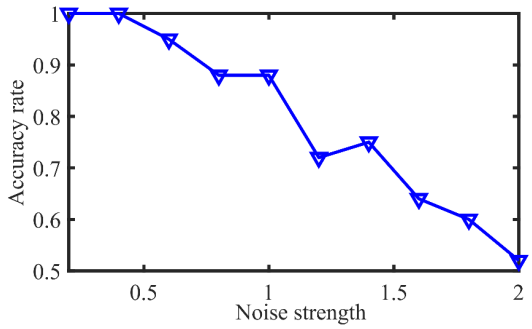

Fig. 16. Accuracy rate of the trained network as a function of the noise strength of the optical digital character.

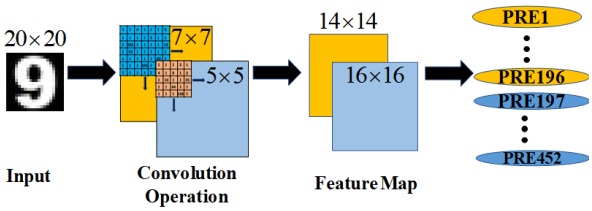

Fig. 17. Schematic of image preprocessing with the convolution operation in the spike encoding phase.

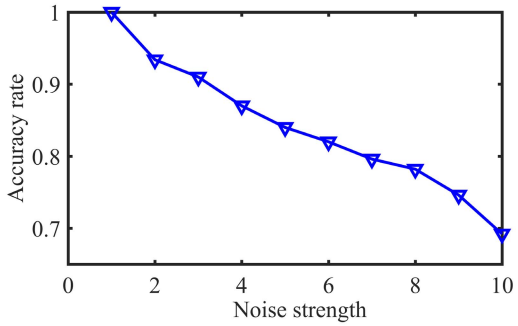

Fig. 18. Accuracy rate of the trained network as a function of the noise strength of the optical digital character when using convolutional precoding of the image.

Fig. 18 shows the results of the testing with the convolution operation in terms of the accuracy rate of the noisy pattern as a function of the noise strength. It can be seen that when $\sigma = 2$, the accuracy rate reaches 0.93, which is much better than that in Fig. 16. Hence, the accuracy rate is significantly improved with the help of using biologically plausible preprocessing with convolution operation.

Without loss of generality, we also consider a case with three prior determined fixed convolutional filters (not shown here). It is found that the accuracy is similar to that shown in Fig. 18. However, note that, with more convolutional filters, the number of PREs is increased, which results in more power consumption of the optical SNN.

The proposed fully VCSEL-based all-optical SNN has several advantages over its counterparts. First, as both the spiking behaviors and STDP learning mechanisms employed in this study are emulated based on different dynamics of VCSELs, an essential advantage of the presented all-optical SNN is high speed, low power consumption, and ease of integration. Second, due to the spatiotemporal design of the spike encoding, the proposed all-optical SNN can implement the classification task without the requirement of lateral inhibition. Third, the

STDP-based supervised training offers biologically plausible learning for the all-optical SNN and could outperform the STDP-based unsupervised learning in all-optical SNN, which shows more powerful capacity in classification task [86].

In this study, only two-layer all-optical SNN is considered. Besides, the output spikes of the POST are spatiotemporally coded and, hence, can act as the input of a next layer, which ensures cascadable spatiotemporal computing in multilayer all-optical SNN. In order to further improve the recognition accuracy of the classification task, the multilayer all-optical SNN or the deep all-optical SNN may be further required [27], [29], [31]–[33], [36], [38]. The hardware-friendly supervised learning algorithm for the multilayer or deep all-optical SNN is still missing, which also deserves additional innovations.

V. Conclusion

In summary, we provided a complete framework, including device, architecture, and algorithm, for computing primitive of bioinspired all-optical SNN on photonic hardware. We have constructed a neuron-synapse self-consistent unified model of all-optical SNN. We show that the system-level model is capable of predicting the various neuron-like dynamics, including the EPSP, excitability, spike latency encoding, as well as the refractory period of a spiking neuron, and the STDP function of a synapse. We finally demonstrate numerically that spike sequence learning and classification task could be successfully realized in the all-optical SNN based on supervised learning according to the ReSuMe rule. Especially, by using spatiotemporal coding for all the input–output and targets, ten POSTs can cooperatively recognize the patterns without the requirement of the lateral inhibition. This work paves the way for the investigation of various physical effects on the neuron-like and synaptic-like dynamics, and the architecture–algorithm codesign and optimization of fully VCSEL-based all-optical SNN.

Note that at the application level, there are various potential application domains in which dedicated neuromorphic photonic systems offer significant advantages in terms of speed and power consumption over conventional computers and electronic neuromorphic systems. These potential application fields include rapid sensory processing, fast autonomous systems, high-performance scientific computing, accelerating the simulation of computational neuroscience models, and large-scale SNN applied to machine learning tasks [58]. Hence, to obtain significant breakthroughs in the neuromorphic photonics, continuing research and development efforts that are required in this interdisciplinary approach involve the device physics, hardware architecture, learning algorithm, photonic integration chip, and neuromorphic applications [2], [40], [58], [67], [100], [101].

References

[1] G. Indiveri and S.-C. Liu, "Memory and information processing in neuromorphic systems," *Proc. IEEE*, vol. 103, no. 8, pp. 1379–1397, Aug. 2015.

[2] K. Roy, A. Jaiswal, and P. Panda, "Towards spike-based machine intelligence with neuromorphic computing," *Nature*, vol. 575, no. 7784, pp. 607–617, Nov. 2019.

[3] W. Maass, "Networks of spiking neurons: The third generation of neural network models," *Neural Netw.*, vol. 10, no. 9, pp. 1659–1671, Dec. 1997.

[4] W. Gerstner and W. M. Kistler, *Spiking Neuron Models: Single Neurons, Populations, Plasticity*. Cambridge, U.K.: Cambridge Univ. Press, 2002.

[5] Z. Mainen and T. Sejnowski, "Reliability of spike timing in neocortical neurons," *Science*, vol. 268, no. 5216, pp. 1503–1506, Jun. 1995.

[6] J. J. Hopfield, "Pattern recognition computation using action potential timing for stimulus representation," *Nature*, vol. 376, no. 6535, pp. 33–36, Jul. 1995.

[7] J. Gautrais and S. Thorpe, "Rate coding versus temporal order coding: A theoretical approach," *Biosystems*, vol. 48, nos. 1–3, pp. 57–65, Nov. 1998.

[8] T. Gollisch and M. Meister, "Rapid neural coding in the retina with relative spike latencies," *Science*, vol. 319, no. 5866, pp. 1108–1111, Feb. 2008.

[9] G.-Q. Bi and M.-M. Poo, "Synaptic modifications in cultured hippocampal neurons: Dependence on spike timing, synaptic strength, and postsynaptic cell type," *J. Neurosci.*, vol. 18, no. 24, pp. 10464–10472, Dec. 1998.

[10] G.-Q. Bi and M.-M. Poo, "Synaptic modification by correlated activity: Hebb's postulate revisited," *Annu. Rev. Neurosci.*, vol. 24, no. 1, pp. 139–166, Mar. 2001.

[11] A. Morrison, M. Diesmann, and W. Gerstner, "Phenomenological models of synaptic plasticity based on spike timing," *Biol. Cybern.*, vol. 98, no. 6, pp. 459–478, Jun. 2008.

[12] S. M. Bohte, J. N. Kok, and H. La Poutré, "Error-backpropagation in temporally encoded networks of spiking neurons," *Neurocomputing*, vol. 48, nos. 1–4, pp. 17–37, Oct. 2002.

[13] R. Gütig and H. Sompolinsky, "The tempotron: A neuron that learns spike timing-based decisions," *Nature Neurosci.*, vol. 9, no. 3, pp. 420–428, Feb. 2006.

[14] A. Kasiński and F. Ponulak, "Comparison of supervised learning methods for spike time coding in spiking neural networks," *Int. J. Appl. Math. Comput. Sci.*, vol. 16, no. 1, pp. 101–113, 2006.

[15] T. Masquelier and S. J. Thorpe, "Unsupervised learning of visual features through spike timing dependent plasticity," *PLoS Comput. Biol.*, vol. 3, no. 2007, p. e31, 2005.

[16] T. Masquelier, R. Guyonneau, and S. J. Thorpe, "Competitive STDP-based spike pattern learning," *Neural Comput.*, vol. 21, no. 5, pp. 1259–1276, May 2009.

[17] F. Ponulak and A. Kasiński, "Supervised learning in spiking neural networks with ReSuMe: Sequence learning, classification, and spike shifting," *Neural Comput.*, vol. 22, no. 2, pp. 467–510, Feb. 2010.

[18] J. J. Wade, L. J. McDaid, J. A. Santos, and H. M. Sayers, "SWAT: A spiking neural network training algorithm for classification problems," *IEEE Trans. Neural Netw.*, vol. 21, no. 11, pp. 1817–1830, Nov. 2010.

[19] R. V. Florian, "The chronotron: A neuron that learns to fire temporally precise spike patterns," *PLoS ONE*, vol. 7, no. 8, Aug. 2012, Art. no. e40233.

[20] A. Mohemmed, S. Schliebs, S. Matsuda, and N. Kasabov, "SPAN: Spike pattern association neuron for learning spatio-temporal spike patterns," *Int. J. Neural Syst.*, vol. 22, no. 4, Aug. 2012, Art. no. 1250012.

[21] J. Humble, S. Denham, and T. Wennekers, "Spatio-temporal pattern recognizers using spiking neurons and spike-timing-dependent plasticity," *Frontiers Comput. Neurosci.*, vol. 6, p. 84, Oct. 2012.

[22] Y. Xu, X. Zeng, and S. Zhong, "A new supervised learning algorithm for spiking neurons," *Neural Comput.*, vol. 25, no. 6, pp. 1472–1511, Jun. 2013.

[23] Y. Xu, X. Zeng, L. Han, and J. Yang, "A supervised multi-spike learning algorithm based on gradient descent for spiking neural networks," *Neural Netw.*, vol. 43, pp. 99–113, Jul. 2013.

[24] Q. Yu, H. Tang, K. C. Tan, and H. Li, "Precise-spike-driven synaptic plasticity: Learning hetero-association of spatiotemporal spike patterns," *PLoS ONE*, vol. 8, no. 11, Nov. 2013, Art. no. e78318.

[25] A. Mohemmed, S. Schliebs, S. Matsuda, and N. Kasabov, "Training spiking neural networks to associate spatio-temporal input–output spike patterns," *Neurocomputing*, vol. 107, pp. 3–10, May 2013.

[26] Q. Yu, H. Tang, K. C. Tan, and H. Li, "Rapid feedforward computation by temporal encoding and learning with spiking neurons," *IEEE Trans. Neural Netw. Learn. Syst.*, vol. 24, no. 10, pp. 1539–1552, Oct. 2013.

[27] I. Sporea and A. Grüning, "Supervised learning in multilayer spiking neural networks," *Neural Comput.*, vol. 25, no. 2, pp. 473–509, Feb. 2013.

[28] J. Wang, A. Belatreche, L. Maguire, and T. M. McGinnity, "An online supervised learning method for spiking neural networks with adaptive structure," *Neurocomputing*, vol. 144, pp. 526–536, Nov. 2014.

[29] Y. Cao, Y. Chen, and D. Khosla, "Spiking deep convolutional neural networks for energy-efficient object recognition," *Int. J. Comput. Vis.*, vol. 113, no. 1, pp. 54–66, May 2015.

[30] P. U. Diehl and M. Cook, "Unsupervised learning of digit recognition using spike-timing-dependent plasticity," *Frontiers Comput. Neurosci.*, vol. 9, p. 99, Aug. 2015.

[31] J. H. Lee, T. Delbruck, and M. Pfeiffer, "Training deep spiking neural networks using backpropagation," *Frontiers Neurosci.*, vol. 10, pp. 1–13, Nov. 2016.

[32] X. Lin, X. Wang, and Z. Hao, "Supervised learning in multilayer spiking neural networks with inner products of spike trains," *Neurocomputing*, vol. 237, pp. 59–70, May 2017.

[33] S. R. Kheradpisheh, M. Ganjtabesh, S. J. Thorpe, and T. Masquelier, "STDP-based spiking deep convolutional neural networks for object recognition," *Neural Netw.*, vol. 99, pp. 56–67, Mar. 2018.

[34] P. Ferré, F. Mamalet, and S. J. Thorpe, "Unsupervised feature learning with winner-takes-all based STDP," *Frontiers Comput. Neurosci.*, vol. 12, Apr. 2018, Art. no. 24.

[35] S. R. Kulkarni and B. Rajendran, "Spiking neural networks for handwritten digit recognition–supervised learning and network optimization," *Neural Netw.*, vol. 103, pp. 118–127, Jul. 2018.

[36] A. Taherkhani, A. Belatreche, Y. Li, and L. P. Maguire, "A supervised learning algorithm for learning precise timing of multiple spikes in multilayer spiking neural networks," *IEEE Trans. Neural Netw. Learn. Syst.*, vol. 29, no. 11, pp. 5394–5407, Nov. 2018.

[37] M. Mozafari, S. R. Kheradpisheh, T. Masquelier, A. Nowzari-Dalini, and M. Ganjtabesh, "First-spike-based visual categorization using reward-modulated STDP," *IEEE Trans. Neural Netw. Learn. Syst.*, vol. 29, no. 12, pp. 6178–6190, Dec. 2018.

[38] A. Tavanaei, M. Ghodrati, S. R. Kheradpisheh, T. Masquelier, and A. Maida, "Deep learning in spiking neural networks," *Neural Netw.*, vol. 111, pp. 47–63, Mar. 2019.

[39] Y. Xu, J. Yang, and X. Zeng, "An optimal time interval of input spikes involved in synaptic adjustment of spike sequence learning," *Neural Netw.*, vol. 116, pp. 11–24, Aug. 2019.

[40] A. Taherkhani, A. Belatreche, Y. Li, G. Cosma, L. P. Maguire, and T. M. McGinnity, "A review of learning in biologically plausible spiking neural networks," *Neural Netw.*, vol. 122, pp. 253–272, Feb. 2020.

[41] C. Mead, "Neuromorphic electronic systems," *Proc. IEEE*, vol. 78, no. 10, pp. 1629–1636, Oct. 1990.

[42] F. Alibart, E. Zamanidoost, and D. B. Strukov, "Pattern classification by memristive crossbar circuits using *ex situ* and *in situ* training," *Nature Commun.*, vol. 4, no. 1, Jun. 2013, Art. no. 2072.

[43] E. Painkras *et al.*, "SpiNNaker: A 1-W 18-core system-on-chip for massively-parallel neural network simulation," *IEEE J. Solid-State Circuits*, vol. 48, no. 8, pp. 1943–1953, Aug. 2013.

[44] B. V. Benjamin *et al.*, "Neurogrid: A mixed-analog-digital multichip system for large-scale neural simulations," *Proc. IEEE*, vol. 102, no. 5, pp. 699–716, May 2014.

[45] P. A. Merolla *et al.*, "A million spiking-neuron integrated circuit with a scalable communication network and interface," *Science*, vol. 345, no. 6197, pp. 668–673, Aug. 2014.

[46] M. Prezioso, F. Merrikh-Bayat, B. D. Hoskins, G. C. Adam, K. K. Likharev, and D. B. Strukov, "Training and operation of an integrated neuromorphic network based on metal-oxide memristors," *Nature*, vol. 521, no. 7550, pp. 61–64, May 2015.

[47] G. W. Burr *et al.*, "Experimental demonstration and tolerancing of a large-scale neural network (165 000 synapses) using phase-change memory as the synaptic weight element," *IEEE Trans. Electron Devices*, vol. 62, no. 11, pp. 3498–3507, Nov. 2015.

[48] S. Park *et al.*, "Electronic system with memristive synapses for pattern recognition," *Sci. Rep.*, vol. 5, no. 1, May 2015, Art. no. 10123.

[49] J. Shen *et al.*, "Darwin: A neuromorphic hardware co-processor based on spiking neural networks," *Sci. China Inf. Sci.*, vol. 59, no. 2, pp. 1–5, Feb. 2016.

[50] R. A. Nawrocki, R. M. Voyles, and S. E. Shaheen, "A mini review of neuromorphic architectures and implementations," *IEEE Trans. Electron Devices*, vol. 63, no. 10, pp. 3819–3829, Oct. 2016.

[51] C. D. Schuman *et al.*, "A survey of neuromorphic computing and neural networks in hardware," 2017, *arXiv:1705.06963*. [Online]. Available: http://arxiv.org/abs/1705.06963

[52] P. Yao *et al.*, "Face classification using electronic synapses," *Nature Commun.*, vol. 8, no. 1, May 2017.

[53] C. Li *et al.*, "Efficient and self-adaptive *in-situ* learning in multilayer memristor neural networks," *Nature Commun.*, vol. 9, no. 1, Jun. 2018, Art. no. 2385.

[54] I. Boybat *et al.*, "Neuromorphic computing with multi-memristive synapses," *Nature Commun.*, vol. 9, no. 1, Jun. 2018, Art. no. 2514.

[55] N. Zheng and P. Mazumder, "Online supervised learning for hardware-based multilayer spiking neural networks through the modulation of weight-dependent spike-timing-dependent plasticity," *IEEE Trans. Neural Netw. Learn. Syst.*, vol. 29, no. 9, pp. 4287–4302, Sep. 2018.

[56] M. Davies *et al.*, "Loihi: A neuromorphic manycore processor with on-chip learning," *IEEE Micro*, vol. 38, no. 1, pp. 82–99, Jan. 2018.

[57] J. Pei *et al.*, "Towards artificial general intelligence with hybrid Tianjic chip architecture," *Nature*, vol. 572, no. 7767, pp. 106–111, Jul. 2019.

[58] B. J. Shastri, A. N. Tait, T. F. de Lima, M. A. Nahmias, H.-T. Peng, and P. R. Prucnal, "Principles of neuromorphic photonics," 2017, *arXiv:1801.00016*. [Online]. Available: http://arxiv.org/abs/1801.00016

[59] A. Hurtado, I. D. Henning, and M. J. Adams, "Optical neuron using polarization switching in a 1550 nm-VCSEL," *Opt. Express*, vol. 18, no. 24, pp. 25170–25176, Nov. 2010.

[60] A. Hurtado, K. Schires, I. D. Henning, and M. J. Adams, "Investigation of vertical cavity surface emitting laser dynamics for neuromorphic photonic systems," *Appl. Phys. Lett.*, vol. 100, no. 10, Mar. 2012, Art. no. 103703.

[61] M. P. Fok, Y. Tian, D. Rosenbluth, and P. R. Prucnal, "Pulse lead/lag timing detection for adaptive feedback and control based on optical spike-timing-dependent plasticity," *Opt. Lett.*, vol. 38, no. 4, pp. 419–421, Feb. 2013.

[62] M. A. Nahmias, B. J. Shastri, A. N. Tait, and P. R. Prucnal, "A leaky integrate-and-fire laser neuron for ultrafast cognitive computing," *IEEE J. Sel. Topics Quantum Electron.*, vol. 19, no. 5, Sep./Oct. 2013, Art. no. 1800212.

[63] F. Selmi, R. Braive, G. Beaudoin, I. Sagnes, R. Kuszelewicz, and S. Barbay, "Relative refractory period in an excitable semiconductor laser," *Phys. Rev. Lett.*, vol. 112, no. 18, May 2014, Art. no. 183902.

[64] Q. Ren, Y. Zhang, R. Wang, and J. Zhao, "Optical spike-timing-dependent plasticity with weight-dependent learning window and reward modulation," *Opt. Express*, vol. 23, no. 19, pp. 25247–25258, Sep. 2015.

[65] B. Gholipour, P. Bastock, C. Craig, K. Khan, D. Hewak, and C. Soci, "Amorphous metal-sulphide microfibers enable photonic synapses for brain-like computing," *Adv. Opt. Mater.*, vol. 3, no. 5, pp. 635–641, Jan. 2015.

[66] R. Toole and M. P. Fok, "Photonic implementation of a neuronal algorithm applicable towards angle of arrival detection and localization," *Opt. Express*, vol. 23, no. 12, pp. 16133–16141, Jun. 2015.

[67] P. R. Prucnal, B. J. Shastri, T. F. de Lima, M. A. Nahmias, and A. N. Tait, "Recent progress in semiconductor excitable lasers for photonic spike processing," *Adv. Opt. Photon.*, vol. 8, no. 2, pp. 228–299, May 2016.

[68] R. Toole *et al.*, "Photonic implementation of spike-timing-dependent plasticity and learning algorithms of biological neural systems," *J. Lightw. Technol.*, vol. 34, no. 2, pp. 470–476, Jan. 15, 2016.

[69] Q. Li, Z. Wang, Y. Le, C. Sun, X. Song, and C. Wu, "Optical implementation of neural learning algorithms based on cross-gain modulation in a semiconductor optical amplifier," *Proc. SPIE*, vol. 10019, Oct. 2016, Art. no. 100190E.

[70] Z. Cheng, C. Ríos, W. H. P. Pernice, C. D. Wright, and H. Bhaskaran, "On-chip photonic synapse," *Sci. Adv.*, vol. 3, no. 9, Sep. 2017, Art. no. e1700160.

[71] S. Y. Xiang *et al.*, "Cascadable neuron-Like spiking dynamics in coupled VCSELs subject to orthogonally polarized optical pulse injection," *IEEE J. Sel. Topics Quantum Electron.*, vol. 23, no. 6, Nov./Dec. 2017, Art. no. 1700207.

[72] T. Deng, J. Robertson, and A. Hurtado, "Controlled propagation of spiking dynamics in vertical-cavity surface-emitting lasers: Towards neuromorphic photonic networks," *IEEE J. Sel. Topics Quantum Electron.*, vol. 23, no. 6, Nov./Dec. 2017, Art. no. 1800408.

[73] Y. Zhang, S. Xiang, J. Gong, X. Guo, A. Wen, and Y. Hao, "Spike encoding and storage properties in mutually coupled vertical-cavity surface-emitting lasers subject to optical pulse injection," *Appl. Opt.*, vol. 57, no. 7, pp. 1731–1737, Mar. 2018.

[74] S. Xiang, Y. Zhang, X. Guo, A. Wen, and Y. Hao, "Photonic generation of neuron-like dynamics using VCSELs subject to double polarized optical injection," *J. Lightw. Technol.*, vol. 36, no. 19, pp. 4227–4234, Oct. 1, 2018.

[75] I. Chakraborty, G. Saha, A. Sengupta, and K. Roy, "Toward fast neural computing using all-photonic phase change spiking neurons," *Sci. Rep.*, vol. 8, no. 1, Aug. 2018, Art. no. 12980.
[76] Y. Zhang, S. Xiang, X. Guo, A. Wen, and Y. Hao, "Polarization-resolved and polarization-multiplexed spike encoding properties in photonic neuron based on VCSEL-SA," *Sci. Rep.*, vol. 8, no. 1, Oct. 2018, Art. no. 16095.
[77] H.-T. Peng, M. A. Nahmias, T. Ferreira de Lima, A. N. Tait, and B. J. Shastri, "Neuromorphic photonic integrated circuits," *IEEE J. Sel. Topics Quantum Electron.*, vol. 24, no. 6, pp. 1–15, Dec. 2018.
[78] S. Y. Xiang, J. K. Gong, Y. H. Zhang, X. X. Guo, A. Wen, and Y. Hao, "Numerical implementation of wavelength-dependent photonic spike timing dependent plasticity based on VCSOA," *IEEE J. Quantum Electron.*, vol. 54, no. 6, Dec. 2018, Art. no. 8100107.
[79] I. Chakraborty, G. Saha, and K. Roy, "Photonic in-memory computing primitive for spiking neural networks using phase-change materials," *Phys. Rev. A, Gen. Phys.*, vol. 11, no. 1, Jan. 2019, Art. no. 014063.
[80] J. K. George *et al.*, "Neuromorphic photonics with electro-absorption modulators," *Opt. Express*, vol. 27, no. 4, pp. 5181–5191, Feb. 2019.
[81] C. Ríos *et al.*, "In-memory computing on a photonic platform," *Sci. Adv.*, vol. 5, no. 2, Feb. 2019, Art. no. eaau5759.
[82] T. F. de Lima *et al.*, "Machine learning with neuromorphic photonics," *J. Lightw. Technol.*, vol. 37, no. 5, pp. 1515–1534, Mar. 1, 2019.
[83] Y. Zhang, S. Y. Xiang, X. Guo, A. Wen, and Y. Hao, "All-optical inhibitory dynamics in photonic neuron based on polarization mode competition in a VCSEL with an embedded saturable absorber," *Opt. Lett.*, vol. 44, no. 7, pp. 1548–1551, Apr. 2019.
[84] J. Feldmann, N. Youngblood, C. D. Wright, H. Bhaskaran, and W. H. P. Pernice, "All-optical spiking neurosynaptic networks with self-learning capabilities," *Nature*, vol. 569, pp. 208–215, May 2019.
[85] A. N. Tait *et al.*, "Silicon photonic modulator neuron," *Phys. Rev. A, Gen. Phys.*, vol. 11, no. 6, Jun. 2019, Art. no. 064043.
[86] S. Xiang, Y. Zhang, J. Gong, X. Guo, L. Lin, and Y. Hao, "STDP-based unsupervised spike pattern learning in a photonic spiking neural network with VCSELs and VCSOAs," *IEEE J. Sel. Topics Quantum Electron.*, vol. 25, no. 6, Nov./Dec. 2019, Art. no. 1700109.
[87] V. A. Pammi, K. Alfaro-Bittner, M. G. Clerc, and S. Barbay, "Photonic computing with single and coupled spiking micropillar lasers," *IEEE J. Sel. Topics Quantum Electron.*, vol. 26, no. 1, Jan./Feb. 2020, Art. no. 1500307.
[88] J. Robertson, E. Wade, Y. Kopp, J. Bueno, and A. Hurtado, "Toward neuromorphic photonic networks of ultrafast spiking laser neurons," *IEEE J. Sel. Topics Quantum Electron.*, vol. 26, no. 1, Jan./Feb. 2020, Art. no. 7700715.
[89] H.-T. Peng *et al.*, "Temporal information processing with an integrated laser neuron," *IEEE J. Sel. Topics Quantum Electron.*, vol. 26, no. 1, Jan./Feb. 2020, Art. no. 5100209.
[90] J. Robertson, T. Deng, J. Javaloyes, and A. Hurtado, "Controlled inhibition of spiking dynamics in VCSELs for neuromorphic photonics: Theory and experiments," *Opt. Lett.*, vol. 42, no. 8, pp. 1560–1563, Apr. 2017.
[91] P. Y. Ma *et al.*, "Simultaneous excitatory and inhibitory dynamics in an excitable laser," *Opt. Lett.*, vol. 43, no. 15, pp. 3802–3805, Aug. 2018.
[92] J. Robertson, T. Ackemann, L. F. Lester, and A. Hurtado, "Externally-triggered activation and inhibition of optical pulsating regimes in quantum-dot mode-locked lasers," *Sci. Rep.*, vol. 8, no. 1, Aug. 2018, Art. no. 12515.
[93] A. Hurtado, I. D. Henning, and M. J. Adams, "Effects of parallel and orthogonal polarization on nonlinear optical characteristics of a 1550 nm VCSOA," *Opt. Express*, vol. 15, no. 14, pp. 9084–9089, Jul. 2007.
[94] M. D. Sánchez, P. Wen, M. Gross, and S. C. Esener, "Rate equations for modeling dispersive nonlinearity in Fabry–Pérot semiconductor optical amplifiers," *Opt. Express*, vol. 11, no. 21, pp. 2689–2696, Oct. 2003.
[95] A. Hurtado and M. J. Adams, "Two-wavelength switching with 1550 nm semiconductor laser amplifiers," *J. Opt. Netw.*, vol. 6, no. 5, pp. 434–441, May 2007.
[96] P. Royo, R. Koda, and L. A. Coldren, "Vertical cavity semiconductor optical amplifiers: Comparison of Fabry–Pérot and rate equation approaches," *IEEE J. Quantum Electron.*, vol. 38, no. 3, pp. 279–284, Mar. 2002.
[97] V. Gauss, A. Hurtado, D. Jorgesen, M. J. Adams, and S. Esener, "Static and dynamic analysis of an all-optical inverter based on a vertical cavity semiconductor optical amplifier (VCSOA)," *Opt. Commun.*, vol. 284, no. 9, pp. 2345–2350, May 2011.
[98] E. S. Bjorlin *et al.*, "Long wavelength vertical-cavity semiconductor optical amplifiers," *IEEE J. Quantum Electron.*, vol. 37, no. 2, pp. 274–281, Feb. 2001.
[99] J. D. Victor and K. P. Purpura, "Nature and precision of temporal coding in visual cortex: A metric-space analysis," *J. Neurophysiol.*, vol. 76, no. 2, pp. 1310–1326, Aug. 1996.
[100] L. Lin, J. Cao, and L. Rutkowski, "Robust event-triggered control invariance of probabilistic Boolean control networks," *IEEE Trans. Neural Netw. Learn. Syst.*, vol. 31, no. 3, pp. 1060–1065, Mar. 2020.
[101] S. Zhu, J. Lu, and Y. Liu, "Asymptotical stability of probabilistic Boolean networks with state delays," *IEEE Trans. Autom. Control*, vol. 65, no. 4, pp. 1779–1784, Apr. 2020.

Shuiying Xiang was born in Ji'an, China, in 1986. She received the Ph.D. degree from Southwest Jiaotong University, Chengdu, China, in 2013.

She is currently a Professor with the State Key Laboratory of Integrated Services Network, Xidian University, Xi'an, China. She has authored or coauthored more than 100 research articles. Her research interests include vertical-cavity surface-emitting lasers, neuromorphic photonic systems, brain-inspired information processing, chaotic optical communication, and semiconductor laser dynamics.

Zhenxing Ren was born in Baoji, China, in 1996. He is currently pursuing the master's degree with Xidian University, Xi'an, China.

His researching interest is machine learning and spiking neural network.

Ziwei Song was born in Jiaozuo, China, in 1996. She is currently pursuing the master's degree with Xidian University, Xi'an, China.

Her researching interest is the vertical cavity surface-emitting lasers and neuromorphic photonic systems.

Yahui Zhang was born in Zhangjiakou, China, in 1993. She is currently pursuing the Ph.D. degree with Xidian University, Xi'an, China.

Her researching interest is the vertical cavity surface-emitting lasers, neuromorphic photonic systems, brain-inspired information processing, and spiking neural networks.

Xingxing Guo was born in Ji'an, China, in 1993. She is currently pursuing the M.S. degree with Xidian University, Xi'an, China.

Her researching interest is the dynamics and applications of semiconductor lasers.

Genquan Han was born in Hengshui, China, in 1979. He received the B.Eng. degree from Tsinghua University, Beijing, China, in 2003, and the Ph.D. degree from the Institute of Semiconductors, Chinese Academy of Sciences, Beijing, in 2008.

He is currently a Professor with Xidian University, Xi'an, China. His current research interests include advanced CMOS, photonics devices, and wide bandgap materials and devices.

Yue Hao (Senior Member, IEEE) was born in Chongqing, China, in 1958. He received the Ph.D. degree from Xi'an Jiaotong University, Xi'an, China, in 1991.

He is currently a Professor with the State Key Discipline Laboratory of Wide Band Gap Semiconductor Technology, School of Microelectronics, Xidian University, Xi'an. His research interests include wide forbidden band semiconductor materials and devices, semiconductor device reliability physics and failure mechanism, and terahertz semiconductor materials and device.